LETTER Communicated by Daniel Tranchina

Populations of Tightly Coupled Neurons: The RGC/LGN System

Lawrence Sirovich
lawrence.sirovich@mssm.edu
Laboratory of Applied Mathematics, Mt. Sinai School of Medicine, New York, NY 10029, U.S.A.

A mathematical model, of general character for the dynamic description of coupled neural oscillators is presented. The population approach that is employed applies equally to coupled cells as to populations of such coupled cells. The formulation includes stochasticity and preserves details of precisely firing neurons. Based on the generally accepted view of cortical wiring, this formulation is applied to the retinal ganglion cell (RGC)/lateral geniculate nucleus (LGN) relay cell system, of the early mammalian visual system. The smallness of quantal voltage jumps at the retinal level permits a Fokker-Planck approximation for the RGC contribution; however, the LGN description requires the use of finite jumps, which for fast synaptic dynamics appears as finite jumps in the membrane potential.

Analyses of equilibrium spiking behavior for both the deterministic and stochastic cases are presented. Green's function methods form the basis for the asymptotic and exact results that are presented. This determines the spiking ratio (i.e., the number of RGC arrivals per LGN spike), which is the reciprocal of the transfer ratio, under wide circumstances. Criteria for spiking regimes, in terms of the relatively few parameters of the model, are presented.

Under reasonable hypotheses, it is shown that the transfer ratio is $\leq$1/2, in the absence of input from other areas. Thus, the model suggests that the LGN/RGC system may be a relatively unsophisticated spike editor. In the absence of other input, the system is designed to fire an LGN spike only when two or more RGC spikes appear in a relatively short time. Transfer ratios that briefly exceed $1/2$ (but are less than 1) have been recorded in the laboratory. Inclusion of brain stem input has been shown to provide a signal that elevates the transfer ratio (Ozaki & Kaplan, 2006). A model that includes this contribution is also presented.

1 Introduction

A convenient hypothesis in modeling neural activity is that neuron populations that perform separate tasks interact through their firing rates. This is

a reasonable assumption in the common circumstance when large numbers of presynaptic neurons converge on the postsynaptic neuron and bring it to discharge. The mean field approximation of Wilson and Cowan (1973) adopts this hypothesis, and a highly refined dynamic form of this appears in the recent population formulations of Knight, Manin, and Sirovich (1996), Knight (2000), and Omurtag, Knight, and Sirovich (2000). However, there are important physiological exceptions to the premise of this scenario, and an example of this is the retinal/lateral geniculate nucleus (LGN) system of the mammalian visual system. In this case, there is ample evidence that precise firing takes place, since as few as one retinal ganglion cell (RGC) may drive one LGN relay cell. Compelling evidence for this "straight-through pathway" appears in a series of pioneering investigations (Bishop, 1953; Cleland, Dubin, & Levick, 1971a, 1971b; Levick, Cleland, & Dubin, 1972). The literature on this topic (Usrey, Reppas, & Reid, 1999; Cleland et al., 1971a, 1971b; Levick et al., 1972; Ruksenas, Fjeld, & Heggelund, 2000) shows a range in the degree and quality of the RGC/LGN coupling, but there is unanimity in the view that few retinal ganglion cells drive a LGN relay cell and that this is efficiently accomplished. Here we adopt a general approach to the description of such tightly coupled interacting populations and apply the formulation to the description of the particular case of RGC/LGN coupling. This will be accomplished within the framework of the population approach that has been put forward in the references already cited.

The origin of the population approach adopted here can be traced to Stein (1965) and the subsequent work by Wilbur and Rinzel (1982, 1983). In those studies, the behavior of single neurons was considered in terms of probable states and resulted in an analytical formulation for the description and evolution of the probability density for single neuron firing. The usefulness and scope of this approach was immensely extended by Knight et al. (1996), Omurtag, Knight, et al. (2000), and Knight (2000). These papers show that the description and evolution of a population of like neurons can be put into the earlier framework. In addition, the theoretical construct was extended to include interactions among the neurons of a population and further to interactions among many populations of neurons. Additional features were explored (Casti et al., 2002; Haskell, Nykamp, & Tranchina, 2001; Nykamp & Tranchina, 2000; Sirovich, 2003; Sirovich, Omurtag, & Lubliner, 2006). Related studies have fleshed out the wide variety of phenomena that are contained in a general population approach (Fusi & Mattia, 1999; Mattia & Del Giudice, 2002; Amit & Brunel, 1997; Gerstner, 1995; Gerstner, van Hemmen, & Cowan, 1996). See Gerstner and Kistler (2002) for a review.

Some doubt has been expressed (Rieke, Warland, van Steveninck, & Bialek, 1997; Usrey & Reid, 1999) in regard to the ability of rate equations to accurately capture complex neuronal activity. In particular, the capacity of rate equations to recruit neuronal synchrony and account for precise firing has been questioned. The former qualm was dealt with for the population formulation in Sirovich et al. (2006), where a wide range of synchronous

behaviors was shown to exist (also see Lytton & Sejnowski, 1991; Ritz & Sejnowski, 1997; Fusi & Mattia, 1999; Brunel & Hakim, 1999; Mattia & Del Giudice, 2002). The study presented here convincingly demonstrates that precise firing can be accurately treated within the framework of the population approach.

2 Formulation

The LGN, a complex structure of the thalamus, is the gateway to many areas of the visual cortex. Most input to the LGN, perhaps as much as 90%, arises from nonretinal sources from higher areas (Sherman & Guillery, 1996). In addition to the massive cortical feedback, collateral LGN neurons from the thalamic reticular nucleus and local interneurons furnish inhibition (Uhlrich, Cucchiaro, & Sherman, 1988). Additionally, the LGN receives input from the brainstem via the parabrachial nucleus (PBN; Ozaki & Kaplan, 2006). By contrast with retinal input to LGN, which is highly specific, the PBN input is globally distributed and appears to be relatively sparse, with perhaps less than 2% of the synapses due to the brainstem (Cucchiaro, Uhlrich, & Sherman, 1988).

Mumford (1991) has theorized that the widespread reciprocity and local LGN circuitry is a dynamic information processing apparatus. It is known that only retinal input elicits firing activity (Kaplan & Shapley, 1984). Section 1 describes the compelling evidence that RGC is directly linked to the LGN. It is also widely agreed that more than 50% of RGC spikes are dropped by the relay cells (Bishop, 1953; Cleland et al., 1971a, 1971b; Levick et al., 1972; Ruksenas et al., 2000; Sincich, Adams, Economides, & Horton, 2007; Andolina, Jones, Wang, & Sillito, 2007; Ozaki & Kaplan, 2006). As a result, it has been opined that this editing feature of LGN relay cells is a source of information processing.

With the exception of a brief later discussion of the PBN, we simplify by restricting attention to the RGC/LGN system. A further simplification, based on sound principles, is introduced by regarding retinal input to LGN as arising from a composite RGC cell, thus avoiding the issue of how few RGC drive an LGN cell. A longer-term goal is the enrichment of this model by the addition of other populations (from LGN and higher areas) to the workings of the basic model developed here.

According to Freed (2005) visual information at the retinal level is well modeled by bipolar cells through glutamate quantal release to RGC; however, it is well known that horizontal and amacrine cells sandwich the bipolar cells (Dowling, 1992). Quantal arrivals activate RGC currents that are encoded as spikes (Fohlmeister & Miller, 1997; Koch et al., 2004; Freed, 2005). The time constant for leakage of current is 1 to 6 ms, more than an order of magnitude smaller than interspike times (Freed, 2005). Therefore, it is reasonable to replace RGC synaptic dynamics by delta function arrivals,

which, in the framework of a simple integrate-and-fire model for the RGC membrane potential, of u, yields

$$\frac{du}{dt} = -\gamma_u u + h_u \sum_k \delta(t - t_k) = -\gamma_u u + I_u \tag{2.1}$$

where $\gamma_u u$ represents leakage current, $\{t_k\}$ denotes the synaptic arrival times, and h_u is the resulting membrane potential jump. Membrane potential, u, has been normalized such that $0 \le u \le 1$, with $u = 0$ representing the resting state and $u = 1$ the threshold for firing, which resets u to zero when reached. Consideration of slower synapses can be found in Haskell et al. (2001) and Fourcaud and Brunel (2002).

The next stage in the visual pathway is the LGN. The preponderance of input to the LGN is from sources other than the retina. RGC arrivals, which can be recorded in the LGN as (slow) S-potentials, are a necessary but not sufficient condition for LGN firing. The prevailing LGN input is largely from higher cortical areas and thus represents feedback, which is thought to deal with information transmission, by editing the RGC input (Uhlrich et al., 1988; Uhlrich, Cucchiaro, Humphrey, & Sherman, 1991; Ozaki & Kaplan, 2006; Andolina et al., 2007)

We regard the retinal ganglion layer as the sole driver of an LGN cell and again resort to an integrate-and-fire model, which for the LGN membrane potential, v, is given by

$$\frac{dv}{dt} = -\gamma_v v + I_v[t; u]. \tag{2.2}$$

RGC input to the LGN is denoted by the functional I_v. The membrane potential v, is also normalized so $v = 0$ is resting and $v = 1$ is the threshold, which is reset to zero when reached. The leakage current is represented by $\gamma_v v$. (We point out that in situations more general than the LGN, the v-neuron receives its own external input and can feed back to the u-neuron.)

The leaky integrate-and-fire models, equations 2.1 and 2.2, represent gross simplification of the richly complex models of retina (Freed, 2005; Fohlmeister & Miller, 1997) and for LGN (McCormick & Huguenard, 1992). Quite generally, the leaky integrate-and-fire model has been shown to be a reliable and serviceable workhorse model for nerve spiking (Kistler, Gerstner, & van Hemmen, 1997; Knight, 2000).

Equations 2.1 and 2.2 represent a coupled dynamical system of equations. The inclusion of stochasticity into dynamics owes its origins to Einstein (1905), Langevin (1906), and others (see Gardiner, 2005). The treatment developed here is presented in this spirit. One variation from the standard stochastic approach is that jumps are not regarded as infinitesimal. This is appropriate since there is compelling evidence that the modeled LGN relay cells experience voltage jumps that cannot be

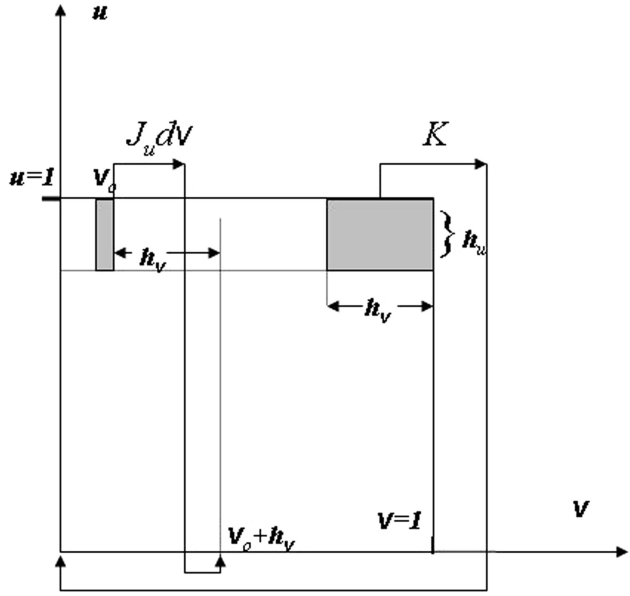

Figure 1: Basic (u, v) domain, a square, for the RGC/LGN system. J_u refers to the flux at the upper threshold and K to the LGN firing rate. As explained in the text, J_v vanishes at $u = 0$ and $u = 1$. An element of flux $J_u(u = 1, v_0)\, dv$ reappears at $u = 0$, $v_0 + h_v$, and all the flux leaving the last subinterval, $(1 - h_v, 1)$ at $u = 1$, which is the LGN firing rate, reappears at the origin. Thus, the total flux exiting at $u = 1$ enters at $u = 0$.

regarded as small. It is also a noteworthy feature of the treatment here that the u and v membrane potentials are fully coupled and that there is no disregard of precise spiking times. Past concern about the ability of the population approach to deal with precise spiking may have been based on a scenario of populations coupled by their firing rates. This is not the case in the investigation here, since we will deal with a single probability density for two membrane voltages, for the RGC and LGN cells. Casti, Hayot, Xiao, and Kaplan (in press) and Haskell et al. (2001) have already dealt with neuron populations involving two state variables. In both cases, the author's interest was focused on synaptic dynamics, and in addition to membrane potential, a conduction or a gating variable appears. While this might eventually prove to be of importance, in the interest of simplicity, we adopt the simplifying assumption of fast synaptics, so that jumps in potential (instead of conductivity jumps) appear. A schematic of the unit square in which the dynamics takes place is shown in Figure 1.

In brief, when a u-neuron lies in the last subinterval $1 - h_u < u < 1$, a synaptic arrival drives the u-neuron to threshold, and it fires. For a

population, the flux is denoted by $J_u dv$. The firing drives the v-neuron from membrane potential v_0 to $v_0 + h_v$. The (u, v)-system is then reset to $(0, v + h)$, unless v is in its last subinterval, $1 - h_v < v < 1$, in which case there is an LGN firing and both neurons are reset at the origin.

We denote the probability of being in the state (u, v) at time t in a volume element $du dv$ by $\rho(u, v, t) du dv$. It then follows that the evolution of ρ is governed by

$$\frac{\partial \rho(u, v, t)}{\partial t} = -\frac{\partial}{\partial u} J_u - \frac{\partial}{\partial v} J_v + J_u(1, v - h_v)\delta(u) + \int_{1-h_v}^{1} J_u(1, v')\, dv' \delta(u)\delta(v). \tag{2.3}$$

The fluxes are

$$J_v(u, v) = -\gamma_v v\rho \;\; \& \;\; J_u(u, v) = -\gamma_u u\rho + \sigma(t) \int_{u-h_u}^{u} \rho(u', v, t)\, du', \tag{2.4}$$

where

$$\sigma(t) = \left\langle \sum_i \delta(t - t_i) \right\rangle_{ensemble} \tag{2.5}$$

denotes the ensemble averaged synaptic arrival rate at the u-neuron (RGC). (See the appendix for the detailed form of equation 2.3.) Both thresholds of the unit square are absorbing boundaries:

$$\rho(1, v, t) = 0 = \rho(u, 1, t). \tag{2.6}$$

Equation 2.3 specifies the evolution of probability, ρ, in terms of its basic fluxes, and further includes the statement that exiting flux at $u = 1$, $J_u(1, v) dv$ reappears at $u = 0$, jumped by h_v, unless v belongs to the last subinterval, $(1 - h_v)$, in which case the v-neurons fire with the net flux,

$$K = \int_{1-h_v}^{1} J_u(1, v)\, dv, \tag{2.7}$$

so that K represents the LGN firing. As seen in equation 2.3 this appears as a flux into the basic square domain at the origin. The derivation of equation 2.3 follows the single unit case (Omurtag, Knight, et al., 2000).

It follows from equation 2.6 that $J_v(u, 0) = J_v(u, 1) = 0$. The remaining net entering flux appears in equation 2.3 as delta function contributions and includes the LGN firing (see equation 2.7). This is exactly balanced by the

exiting flux $\int_0^1 J_u(1, v)\, dv$, and the formal integration of equation 2.3 over the unit square of Figure 1 yields

$$\frac{\partial}{\partial t} \int_o^1 du' \int_o^1 dv' \rho(u', v', t) = 0; \tag{2.8}$$

conservation of probability is respected. As another check of equation 2.3, we observe that the marginal distribution,

$$\rho_1(u, t) = \int_0^1 dv' \rho(u, v', t), \tag{2.9}$$

satisfies

$$\frac{\partial \rho_1(u, t)}{\partial t} = \frac{\partial}{\partial u} \left\{ (\gamma_u u \rho_1(u, t)) - \int_{u-h_u}^{u} \rho_1(u', t)\, du' \right\} + \sigma(t)\delta(u) \int_{1-h_u}^{1} \rho_1(u', t)\, du', \tag{2.10}$$

the one neuron population equation derived in Omurtag, Knight, et al. (2000) and discussed in a variety of frameworks (Knight, Omurtag, & Sirovich, 2000; Omurtag, Kaplan, Knight, & Sirovich, 2000; Sirovich, Knight, & Omurtag, 2000; Sirovich, 2003; Sirovich et al., 2006).

The presence of delta functions in equation 2.3 at the boundaries $u = 0$ and $v = 0$ indicates population accumulations at such locations. Such neurons are dislodged by synaptic arrivals at the arrival rate. In the course of numerical simulations, the presence of delta functions can lead to some inaccuracies. It therefore is of practical significance that the solution to equation 2.3, on theoretical grounds, can be decomposed as follows,

$$\rho = A(v, t)\delta(u) + B(u, t)\delta(v) + C(t)\delta(u)\delta(v) + \hat{\rho}(u, v, t), \tag{2.11}$$

with $\hat{\rho}$ free of delta function factors (Sirovich, 2003). As shown in the appendix, this results in a system of four coupled differential equations, so that delta functions never need to be given a coarse grain approximation.

We reiterate our earlier remark that equation 2.3 is a consequence of regarding equations 2.1 and 2.2, as a single unit, and represents a novel form of stochastic dynamics. In the limit of small jumps, it subsumes the common diffusion approximation for stochasticity, one aspect of which is considered next.

Freed (2005) reports that the number of quantal arrivals needed to produce an RGC spike can vary over a wide range, depending on how natural the stimulus is. In his model, these events occur asynchronously and are

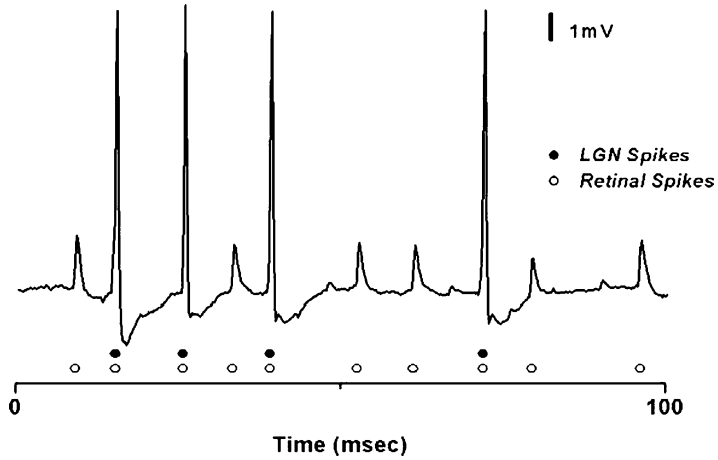

Figure 2: Extracellular (differentiating) record of S-potential/spike from an LGN relay cell (Ozaki & Kaplan, 2006). Note that LGN spikes always coincide with S-potentials.

modeled by Poisson arrivals. According to Freed, about 10 jumps, h_u, are needed for the RGC to reach threshold under normal conditions (under extreme experimental conditions, this number increases by more than an order of magnitude). From this, it follows that we can reasonably regard h_u as small enough to adopt the diffusion approximation, although at $h_u = 0.1$ this may be a concern.

By contrast, as explained in section 1, the LGN cell receives a highly synchronized assembly of arrivals, possibly from as few as one RGC, resulting in a substantial voltage jump, known as an S potential (see Usrey et al., 1999, for a review). This is illustrated in Figure 2, and from this we might suppose $h_v > \frac{1}{2}$, although on a cautionary note, it should be noted that Figure 2 is an extracellular recording. The strong coupling of retinal ganglion and relay cells is underlined by this figure.

2.1 RGC/LGN System. From the above discussion it appears appropriate that we consider equations 2.10 and 2.11 for $h_u \approx 0$ and $h_v = h$ bounded away from zero. When this is done, it is found that A and C in equation 2.11 can be taken as zero, so that

$$\rho = B(u,t)\delta(v) + \hat{\rho}(u,v,t), \tag{2.12}$$

and if *current* is defined as

$$s = h_u\sigma \tag{2.13}$$

and *diffusivity* as

$$\mu = \frac{1}{2} s h_u, \tag{2.14}$$

then expanding under the integral through order h_u^2 yields

$$\frac{\partial}{\partial t} B(u,t) = \frac{\partial}{\partial u}\left\{(\gamma_u u - s)B + \mu \frac{\partial B}{\partial u}\right\} \tag{2.15}$$

and

$$\frac{\partial}{\partial t}\hat{\rho}(u,v,t) = \frac{\partial}{\partial u}\left\{(\gamma_u u - s)\hat{\rho} + \mu \frac{\partial}{\partial u}\hat{\rho}\right\} + \frac{\partial}{\partial v}(\gamma_v v \hat{\rho}). \tag{2.16}$$

The flux J_u, equation 2.4, to this approximation becomes

$$J_u = \left\{(s - \gamma_u u)B - \mu \frac{\partial B}{\partial u}\right\}\delta(v) + \left\{(s - \gamma_u u)\hat{\rho} - \mu \frac{\partial \hat{\rho}}{\partial u}\right\}, \tag{2.17}$$

and the absorbing boundary conditions, equation, 2.6 are consistent with

$$B(1,t) = 0; \quad \hat{\rho}(1,v,t) = 0 = \hat{\rho}(u,1,t). \tag{2.18}$$

As h_u has exited the problem at this point we will drop the subscript from h_v. There is no current source for $\hat{\rho}$ when $v < 0$, whence $\hat{\rho}(u, v < 0) = 0$, and the flux boundary condition becomes

$$\begin{aligned} J_u(0,v) = &-\mu \int_{1-h}^{1} \frac{\partial \hat{\rho}}{\partial u}(1,v')\, dv' \delta(v) \\ &- \left\{\mu \frac{\partial B}{\partial u}(1,t)\delta(v-h) + \mu \frac{\partial \hat{\rho}}{\partial u}(1, v-h, t)\right\}, \end{aligned} \tag{2.19}$$

where the bracketed term is valid for $v \geq h$. It should be noted that the coefficient of $\delta(v)$ in equation 2.19 is K, the firing rate of the LGN relay cell (see Figure 1), and thus it is the input boundary condition at $u = 0$ for equation 2.15, while the remaining condition is given by the first term in equation 2.18.

It is easily seen that the integral of equation 2.12 over the domain $0 \leq u, v \leq 1$ is conserved and that the marginal distribution

$$\rho_1(u,t) = B(u,t) + \int_0^1 dv' \hat{\rho}(u,v',t) \tag{2.20}$$

satisfies

$$\frac{\partial}{\partial t}\rho_1(u,t) = \frac{\partial}{\partial u}\left\{(\gamma_u u - s)\rho_1 + \mu\frac{\partial \rho_1}{\partial u}\right\}. \tag{2.21}$$

Thus, the marginal distribution $\rho_1(u,t)$ satisfies the same equation, 2.15, as $B(u,t)$. To contrast the two cases, we observe that the $B(u,t)$ equation is driven by the v-neuron firing rate, while the $\rho_1(u,t)$ equation is driven essentially by external current.

3 Deterministic Case

For conceptual reasons and for later analysis, it is useful to first consider the nonstochastic case. The ensemble averaged form of equation 2.1 is

$$\frac{du}{dt} = -\gamma u + s, \tag{3.1}$$

where for present purposes, we take s to be a constant current. If $\{\tau_j\}$ denote the firing times of equation 3.1, then

$$\frac{dv}{dt} = -\gamma v + h\sum_j \delta(t - \tau_j) \tag{3.2}$$

describes the behavior of the v-neuron. Note that we have taken $\gamma_u = \gamma_v = \gamma$, which is attractive for reasons of exposition since trajectories of equations 3.1 and 3.2 are straight lines in the (u, v)-plane. (An estimate for the retinal leakage time, γ_u^{-1}, is 50 msec (Fohlmeister & Miller, 1997) and for the relay cell leakage time γ_v^{-1} it is 10 msec (Ozaki & Kaplan, 2006).) To see this, it is sufficient to consider

$$\frac{du}{dv} = \frac{s/\gamma - u}{v}, \tag{3.3}$$

which has the linear solution

$$\frac{s/\gamma - u}{s/\gamma - u_0} = \frac{v}{v_0}, \tag{3.4}$$

where(u_0, v_0) are the initial conditions. (For $\gamma_u \neq \gamma_v$, the trajectories follow a power law.)

We restrict attention to $s/\gamma > 1$; otherwise, the deterministic u-neuron does not fire. The details of the dynamics 3.1 and 3.2 are revealed by considering the reset state $(u_0, v_0) = (0, 0)$ as the initial state.

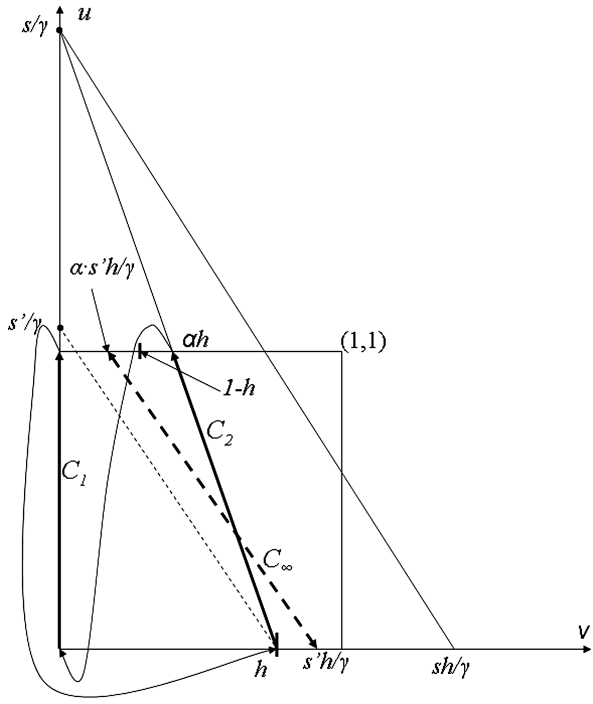

Figure 3: Heavy lines C_1 and C_2 depict $sh/\gamma > 1$. C_1, C_2 and their connecting lines form a limit cycle. For $s'h/\gamma < 1$, C_∞ is a limit cycle.

The system point for the two-neuron system makes a sequence of passages from the bottom to the top of the square, as shown in Figure 3. We call its coordinate at the nth exit (at $u = 1$) $\bar{v}_n$, and its immediate reappearance (at $u = 0$) $\underline{v}_{n+1} = \bar{v}_n + h$. Thus, reference abscissa values carry an overbar ($\bar{v}$) at $u = 1$ and an underbar ($\underline{v}$) at $u = 0$.

It is clear from equation 3.4 (or equations 3.1 and 3.2) that all trajectories would terminate in $(s/\gamma, 0)$ in the absence of the threshold condition at $u = 1$. Starting at $u = 0$ and $\underline{v}_0 = 0$, the trajectory ascends the u axis, and reaches $u = 1$, at $\bar{v}_0 = 0$ indicated in Figure 3 by the heavy line C_1, then jumps to $\underline{v}_1 = h, u = 0$, and then proceeds along the heavy line C_2 to $\bar{v}_1 = \alpha h$, at $u = 1$, where

$$\alpha = \frac{s/\gamma - 1}{s/\gamma} = 1 - \frac{\gamma}{s}. \tag{3.5}$$

In general

$$\bar{v}_j = T\underline{v}_j = \alpha\underline{v}_j, \tag{3.6}$$

where T is the transformation dictated by similar triangles in Figure 3, and

$$\underline{v}_{j+1} = T_h \bar{v}_j = \bar{v}_j + h, \tag{3.7}$$

where T_h is the translation, by h, operator. If these transformations are applied to the seed $(0, 0)$, this yields

$$\underline{v}_j = h \sum_{k=0}^{j-1} \alpha^k = h \frac{1-\alpha^j}{1-\alpha}, \quad j \geq 1 \tag{3.8}$$

with the crossing points at $u = 1$ given by

$$\bar{v}_j = \alpha h \sum_{k=0}^{j-1} \alpha^k = \alpha h \frac{1-\alpha^j}{1-\alpha}, \quad j \geq 1. \tag{3.9}$$

In the infinite limit, equation 3.9 yields

$$\underline{v}_\infty = \frac{sh}{\gamma} \tag{3.10}$$

and

$$\bar{v}_\infty = \alpha \underline{v}_\infty = h\left(\frac{s}{\gamma} - 1\right), \tag{3.11}$$

which confirms $T_h \bar{v}_\infty = \underline{v}_\infty$. It is clear that the LGN neuron will not fire unless $sh/\gamma > 1$ and that the LGN cell is silent for

$$\frac{sh}{\gamma} < 1. \tag{3.12}$$

Both cases are depicted in Figure 3. Under condition 3.12, the LGN does not fire, and only the limiting case is shown, in which case the RGC fires at the frequency

$$\nu = -\gamma / ln(1 - \gamma/s), \tag{3.13}$$

obtained by integrating equation 3.1 to $u = 1$. In fact, for this case, equation 3.12, the trajectory C_∞ is a limit cycle of the system, taking a time $1/\nu$ to go from $\underline{v}_\infty$ to $\bar{v}_\infty$ and zero time to return to $\underline{v}_\infty$.

To see that C_∞ is attracting, observe that from equation 3.12,

$$1 - \gamma/s < 1 - h, \tag{3.14}$$

and therefore the extreme case of a seed at $(u, v) = (0, 1)$ passes to the left of $1 - h$ at $u = 1$, and after N steps, it is at $\underline{v}_N = h(1 + \alpha + \alpha^2 + \cdots + \alpha^N) + \alpha^N$, which clearly tends to $\underline{v}_\infty$ for $N \uparrow \infty$.

If

$$\frac{sh}{\gamma} > 1 \tag{3.15}$$

$\underline{v}_\infty$, equation 3.10, is greater than unity; hence, the v-cell fires in a finite number of steps. For the case shown in Figure 3, the v-cell fires at the second step, and C_1 and C_2 also constitute a limit cycle.

The ratio of LGN firing to RGC arrivals is known in the physiological literature as the transfer ratio (Ruksenas et al., 2000; Ozaki & Kaplan, 2006). It is also convenient to consider the reciprocal of the transfer ratio, which informs us of the number of RGC arrivals, and hence the number of jumps, h, required to yield an LGN firing. We will refer to this as the spiking ratio. The first firing always occurs at $(u, v) = (1, 0)$. At the next exit, the potential is $\bar{v}_1$, and if $v_1 \geq 1 - h$ the spiking ratio is 2, and at the nth firing brings the potential to

$$\bar{v}_n = \alpha^{n-1}\bar{v}_1 + h\left(\frac{1 - \alpha^n}{1 - \alpha}\right) - h. \tag{3.16}$$

For latter purposes, we leave $\bar{v}_1$ open, but if $\bar{v}_1 = \alpha h$, we recover equation 3.9. Since the condition for firing is that $\bar{v}_n = 1 - h$, we obtain

$$n(\bar{v}_1) = ln\left(\frac{1 - \gamma/sh}{1 - \bar{v}_1/(h(s/\gamma - 1))}\right) \Big/ ln(1 - \gamma/s), \tag{3.17}$$

for the number of jumps to firing. In the present context, only integer values make sense, and it is understood that $n(\bar{v}_1)$ should be rounded up (see Figure 7). Thus, if $h > 1/2$, we can have $n = 2$, and the LGN cell can fire at the same rate as the RGC only if $h \geq 1$.

A case of interest, to be considered in more detail, is

$$h > 1/2.$$

In this case, if

$$\frac{s}{\gamma} > h/(2h - 1), \tag{3.18}$$

the v-cell fires after every second u-cell arrival, the transfer ratio is $1/2$, and this is roughly what might be seen in the laboratory (see Figure 2; Ozaki & Kaplan, 2006).

4 Equilibrium Solution

In the case of equilibrium, $\partial/\partial t = 0$, equation 2.16, becomes

$$\frac{\partial}{\partial u}\left\{(\gamma u - s)\hat{\rho} + \mu\frac{\partial}{\partial u}\hat{\rho}\right\} + \frac{\partial}{\partial v}(\gamma v\hat{\rho}) = 0, \tag{4.1}$$

and the marginal distribution, equation 2.20, satisfies

$$\frac{\partial}{\partial u}\left\{(\gamma u - s)\rho_1 + \mu\frac{\partial \rho_1}{\partial u}\right\} = 0, \tag{4.2}$$

so that RGC flux is conserved. Thus,

$$(\gamma u - s)\rho_1 + \mu\frac{\partial \rho_1}{\partial u} = -J_o, \tag{4.3}$$

where the constant J_o is the firing rate of the RGC population per unit neuron. The equilibrium form of equation 2.15 has the similar first integral,

$$(\gamma u - s)B + \mu\frac{\partial B}{\partial u} = -K, \tag{4.4}$$

again indicating a conservation of flux, where K is the firing rate of the LGN relay cell population. Both equations 4.3 and 4.4 may be explicitly solved in terms of quadratures (see equation 5.2), and we denote the solution, equation 4.4, by $B(u, K)$ and therefore $\rho_1 = B(u, J_o)$ is the solution to equation 4.3. The marginal distribution satisfies

$$\int_0^1\int_0^1 du\,dv\,\rho(u, v) = \int_0^1 du\,\rho_1(u)\,du = 1, \tag{4.5}$$

and with $\rho_1 = B(u, J_o)$ on hand from equation 4.3, this leads to the determination of $J_o = J_o(s, \gamma)$ (see Figure 4 and equation 5.7 below). On the other hand, in general $B(u, K)$ does not satisfy an a priori normalization condition, and the full problem must be considered before K can be determined.

In addition to the absorbing boundary conditions, $B(1) = 0$ & $\hat{\rho}(1, v) = \hat{\rho}(u, 1) = 0$, we have the flux conditions, equation 2.19,

$$sB(0) - \mu\frac{\partial B}{\partial u}(0) = -\mu\int_{1-h}^1 \frac{\partial \hat{\rho}}{\partial u}(1, v')\,dv' = K. \tag{4.6}$$

and

$$s\hat{\rho}(0,v)-\mu\frac{\partial\hat{\rho}}{\partial u}(0,v)=\begin{cases}0; & 0\le v<h\\ -\mu\dfrac{\partial B}{\partial u}(1,t)\delta(v-h)-\mu\dfrac{\partial\hat{\rho}}{\partial u}(1,v-h); & v\ge h\end{cases} \tag{4.7}$$

which couples equations 4.1 and 4.4.

4.1 Small Diffusion: $\mu \downarrow 0$. To obtain an analytical grip on the analysis, we pursue the $\mu \downarrow 0$ limit, which was justified by earlier remarks. From equation 4.6, it then follows that

$$B(0)\approx\frac{K}{s}, \tag{4.8}$$

and to lowest order, the formal outer solution of equation 4.4, $\mu = 0$, is

$$B=\frac{K}{s-\gamma u}. \tag{4.9}$$

In the neighborhood of $u = 1$, there is a boundary layer of $O(\mu)$, and a uniform solution to the boundary layer approximation of equation 4.4 is for $s > \gamma$,

$$B(u:K)=\frac{K}{s-\gamma u}\left(1-e^{-(s-\gamma)(1-u)/\mu}\right). \tag{4.10}$$

Thus, for $(1-u)/\mu$ fixed and $\mu \downarrow 0$, we get the boundary layer solution, and for u fixed and $\mu \downarrow 0$, we get the outer solution, equation 4.9. By the same token, the solution for ρ_1 is $B(u : J_0)$. From the normalization condition, equation 4.5, applied to the latter, we obtain

$$J_0=\nu\left(1-\frac{\mu\nu}{(s-\gamma)^2}\right)^{-1}, \tag{4.11}$$

where ν is given by equation 3.13. Thus, the presence of the boundary layer in effect reduces the firing threshold, so that the firing rate is slightly increased.

The determination of $\hat{\rho}$ from equation 4.1 follows in a similar fashion. If $\mu = 0$ in equation 4.1, we see that the (sub)characteristics (Cole, 1968) are just the trajectories of the deterministic case considered in section 3. For

initial data $\hat{\rho}_0(v)$ at $u = 0$, and $v \geq h$, the outer solution, $\mu = 0$, to equation 4.1 is

$$\hat{\rho}(u, v) = \frac{\hat{\rho}_0(v/(1 - \gamma u/s)}{(1 - \gamma u/s)^2}, \tag{4.12}$$

which since $\hat{\rho}$ must vanish at $u = 1$, requires a boundary layer, of $O(\mu)$, for $u \approx 1$. Proceeding as above, we obtain the uniformly valid solution,

$$\hat{\rho}(u, v) \approx \frac{\hat{\rho}_0(v/(1 - \gamma u/s)}{(1 - \gamma u/s)} \frac{\left(1 - e^{-(s-\gamma)(1-u)/\mu}\right)}{(s - \gamma u)}. \tag{4.13}$$

To implement these considerations, we consider the case depicted in Figure 3: when $h > 1/2$. If $sh/\gamma > 1$ is sufficiently large, the trajectory is the limit cycle made up of C_1 and C_2 shown in the Figure 3. From equation 4.7, the initial condition is

$$\hat{\rho}(0, v) = -\frac{\mu}{s} \frac{\partial B(1 : K)}{\partial u} \delta(v - h) = \frac{K}{s} \delta(v - h) \tag{4.14}$$

since $\mu \partial \hat{\rho}(0, v)/\partial u$ is negligible. Hence, from equation 4.13, the uniformly valid solution is

$$\hat{\rho}(u, v) = \delta(v - h(1 - \gamma u/s)) B(u : K). \tag{4.15}$$

K may be determined in a number of ways, all of which yield

$$K = \frac{J_o}{2}, \tag{4.16}$$

where J_o is given by equation 4.11. If $sh/\gamma < 1$ ($h > \frac{1}{2}$) as Figure 3 indicates $K = 0$, that is, independent of the initial state, the system seeks out the limit cycle denoted by C_∞ ($\underline{v}_\infty \rightleftarrows \bar{v}_\infty$).

5 Improved Asymptotics

The boundary layer analysis of the previous section has several shortcomings, one of which is that it lacks validity when $s \approx \gamma$, and smaller. To rectify this and other deficiencies, mentioned below, observe that the one-dimensional flux satisfies

$$(s - \gamma u)\phi - \mu \frac{\partial \phi}{\partial u} = s, \tag{5.1}$$

gotten by substituting $\phi = s\rho_1/J_o$ in equation 4.3. For $\phi(1) = 0$ this has the solution (Brunel & Hakim, 1999; Sirovich et al., 2000)

$$\phi(u) = \frac{s}{\mu} \exp\left[-\left(\frac{\gamma u^2}{2\mu} - \frac{su}{\mu} \right) \right] \int_u^1 \exp\left[\frac{\gamma w^2}{2\mu} - \frac{sw}{\mu} \right] dw. \tag{5.2}$$

We observe that

$$-\mu \frac{\partial \phi}{\partial u}\bigg|_{u=1} = s, \tag{5.3}$$

and to lowest order in μ,

$$\phi(u = 0) \approx 1. \tag{5.4}$$

Thus, the (exact) solution (but with K still open) of equation 4.4 is

$$B = \frac{K}{s}\phi(u). \tag{5.5}$$

Similarly, the marginal distribution, equation 4.3, has the solution

$$\rho_1(u) = \frac{J_o}{s}\phi(u). \tag{5.6}$$

(As is easily seen, equation 5.5 yields equation 4.13 for $\mu \downarrow 0$ when $u \approx 1$.) As mentioned earlier, imposition of the normalization (see equation 4.4) leads to the determination of J_o (Sirovich et al., 2000):

$$\frac{1}{J_o} = -\mu\gamma \int_0^1 du\ ln\ u \Big\{ (\gamma(1-u) - s) \exp\left[-\left(\frac{\gamma u^2}{2\mu} - \frac{u}{\mu}(\gamma - s) \right) \right] - (u\gamma - s) \exp\left[\frac{\gamma u^2}{2\mu} - \frac{su}{\mu} \right] \Big\}. \tag{5.7}$$

The RGC firing rate with diffusion, J_o, is plotted in Figure 4, along with the nonstochastic rate $\nu(s)$ (see equation 3.13).

Clearly the stochastic nature of diffusion in the u-direction should mitigate the abrupt loss of firing that occurs at $s = \gamma$ in the expression for $\nu(s)$, equation 3.13. Also the simple boundary layer analysis above indicates an abrupt loss of LGN firing for $sh/\gamma = 1$, equation 3.12, and it might be supposed that the presence of RGC diffusion would be mitigating and allow occasional sparsely spaced LGN impulses in this range. The simple boundary layer analysis is not sufficiently refined to account for the vertical diffusion of $\delta(v - h)$ as it evolves across the unit square from

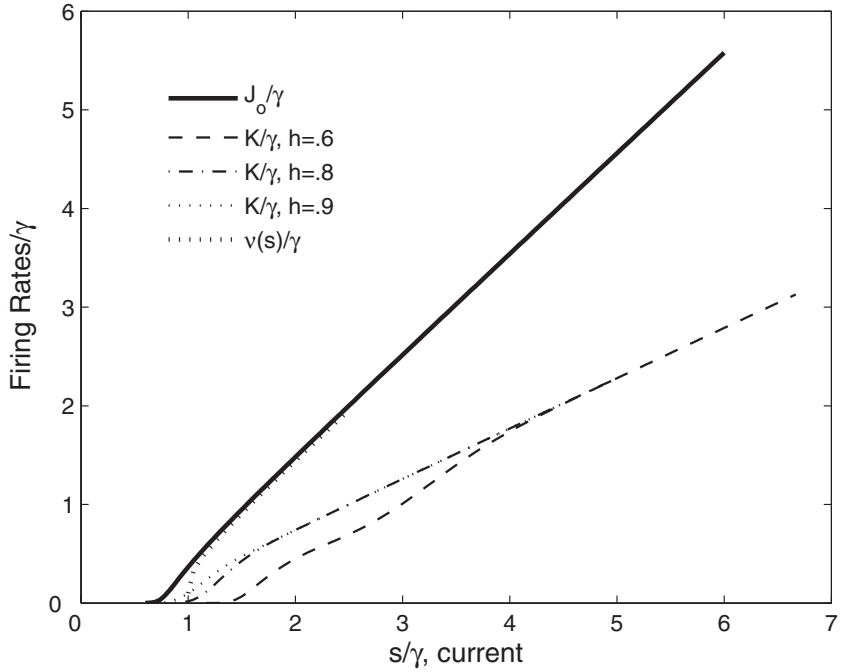

Figure 4: J_o represents the RGC firing rate given by equation 5.7, for $\gamma^{-1} = 50$ msec. K, the LGN firing rate, is calculated from equation 6.8. Note that this asymptotes to $J_o/2$ see equation 4.16.

$u = 0$ to $u = 1$, under which action the v-neuron could fire, $K \neq 0$, albeit infrequently.

On the other hand $\phi(u)$, equation 5.2, is an exact solution of 4.1, which satisfies the exact boundary condition equation 5.3, and for μ small has a convenient approximation (see equation 5.4). With this in mind, based on the form of equation 4.15, we seek an approximate solution of equation 4.1 in the form

$$\hat{\rho} = \tilde{D}(u, v)\phi(u). \tag{5.8}$$

If equation 5.8 is substituted into equation 4.1, we obtain

$$\phi\left[\frac{\partial}{\partial u}\left(\left(u - \frac{s}{\gamma}\right)\tilde{D}\right) + \frac{\mu}{\gamma}\frac{\partial^2 \tilde{D}}{\partial u^2} + v\frac{\partial \tilde{D}}{\partial v}\right] + \left\{2\frac{\mu}{\gamma}\frac{\partial \phi}{\partial u}\frac{\partial \tilde{D}}{\partial v}\right\} = 0. \tag{5.9}$$

In a moment we will argue that the term in the curly brackets in equation 5.9 is small and thus that we need only consider the solution for vanishing square brackets, which we denote by D,

$$\frac{\partial}{\partial u}\left\{(u - s/\gamma)D + \frac{\mu}{\gamma}\frac{\partial}{\partial u}D\right\} + v\frac{\partial D}{\partial v} = 0. \tag{5.10}$$

Under the transformation

$$ln\ v = -t'; \quad x = u - \frac{s}{\gamma}, \tag{5.11}$$

equation 5.10 becomes

$$\frac{\partial D}{\partial t'} = \frac{\partial}{\partial x}\left(xD + \frac{\mu}{\gamma}\frac{\partial D}{\partial x}\right), \tag{5.12}$$

an Ornstein-Uhlenbeck equation (Risken, 1996; Gardiner, 2005). For present purposes, a useful solution of equation 5.10 is

$$D(u, v : v_0)\begin{cases} = \dfrac{s}{\gamma v_0}\dfrac{\exp\left[-\left\{u - \frac{s}{\gamma}\left(1 - \frac{v}{v_o}\right)\right\}^2 / 2\mu\left(1 - \frac{v^2}{v_0^2}\right)\gamma^{-1}\right]}{\sqrt{2\mu\pi\left(1 - \frac{v^2}{v_0^2}\right)/\gamma}}, & v < v_0. \\ \equiv 0, v \geq v_0 \end{cases} \tag{5.13}$$

That $D \equiv 0$ for $v > v_0$ follows from t', in equation 5.12, being time-like. (It is of more than passing interest that $\hat{\rho} = D/v$ is an exact solution of equation 4.1.) For $\mu \downarrow 0$, equation 5.13 becomes

$$D(u, v : v_0) \to \delta(v - v_0(1 - \gamma u/s)). \tag{5.14}$$

Thus the notation of equation 5.13 indicates that $v = v_0$ is the location of the delta function at $u = 0$. Equation 5.14 also shows that equation 5.10, for $v_0 = h$, tends to equation 4.15. (Equation 5.13 comes from an infinite domain analysis, and some fine print is in order. For $u = 0$, equation 5.13 is not gaussian, but for μ small, it retains the delta function property, and the integral over $0 < v < 1$ is close to unity. With varying small error, this is true for $0 \leq u \leq 1$. Additionally, due to diffusion, equation 5.13 introduces a back flux to $u = 0$. This, however, is negligible.)

For the case of small μ, the curly bracketed term in equation 5.10 is small, $O(\mu)$, except in the boundary layer where $\mu\frac{\partial \phi}{\partial u}$ is $O(1)$. However, in the boundary layer, D is a narrow gaussian, equation 5.14, for $\mu \downarrow 0$, and $\frac{\partial D}{\partial v}$, which appears in the curly brackets, has a zero crossing at $v = v_0(1 - \frac{\gamma}{s})$, which gives some basis for neglecting this term. Alternately, when $u \to 1$,

$\frac{\partial D}{\partial v}$ represents a dipole of flux, and its integral is negligible. In any case there is a basis for the neglect of the bracketed term in equation 5.9. And in the following we take

$$\hat{\rho}(u, v) \approx D(u, v : v_0)\phi(u) \tag{5.15}$$

as the (approximate) Green's function solution of equation 4.1, that is, it tends to a delta function at $u = 0, v = v_0$. The use of this approximation allows for an explicit formulation of the problem, which is solved using numerical methods, in the next section. In an effort to provide insight into the nature of the dynamics, we first present a heuristic discussion relating the deterministic case to the computational results.

The Green's function see equation 5.15 describes how a source, at $u = 0$ and $v = v_0$, diffuses in the u-direction. We recall that the LGN firing rate, K, produces a delta function of the same strength at $(u, v) = (0, 0)$. This later shows up as a flux source $K\delta(v - h)$, at $u = 0$. Recall that in the deterministic case, the LGN neuron will fire if the next trajectory (subcharacteristic of equation 4.1) crosses $u = 1$ at $v > 1 - h$. If not, and $sh/\gamma > 1$, it will fire after some number of jumps across the computational square, equation 3.17, while if $sh/\gamma < 1$, the LGN never fires.

To envision how this picture is modified by stochasticity, it is useful for the moment to imagine an iterative process leading to equilibrium. At the first stage, the source $K\delta(v - h)$ evolves according to equation 5.15 and appears at $u = 1$ as a flux shown in Figure 5 as a continuous, gaussian-like curve. The net flux, at $u = 1$, to the right of $v = 1 - h$, generates LGN firing, which appears at the origin. The flux to the left of $v = 1 - h$, shown as a dashed curve in the figure, is then mapped to $u = 0$, and $v > h$, from equation 4.7, also shown as a dashed curve in the figure. This last portion of influx at $u = 0$ then evolves via the Green's function, equation 5.15, into the dashed curve at $u = 1, v > 1 - h$ shown in the figure. The result of these early stages as sketched in Figure 5 depicts the case when the deterministic trajectory crosses $u = 1$ to the right of $1 - h$. This process can be repeated indefinitely and, as indicated in the next section, leads to the exact solution.

Figure 6 shows four cases of calculations of the probability density as generated by the precise formulation given in the next section. At the upper left $\hat{\rho}(u, v)$, for $sh/\gamma = 3$, is shown. In this case, as will be seen, most of the flux at $u = 1$ is to the right of $1 - h$. However, there is an imperceptible ripple that emanates from the neighborhood of $v = 1$, which can be seen in the numerics. In the context of the deterministic case, this corresponds to neurons with a spiking ratio of 3. This slight bimodality is just perceptible at $sh/\gamma = 2.28$ and becomes pronounced for $sh/\gamma = 1.56$. The enhancement of the second bump reflects the effect of an increasing number of neurons that require many jumps, equation 3.17, for the LGN cell to fire. It is also clear that the strength of the delta function at $u = 0, v = h$, which reflects the LGN firing rate, diminishes as sh/γ decreases. In the final frame at the lower right,

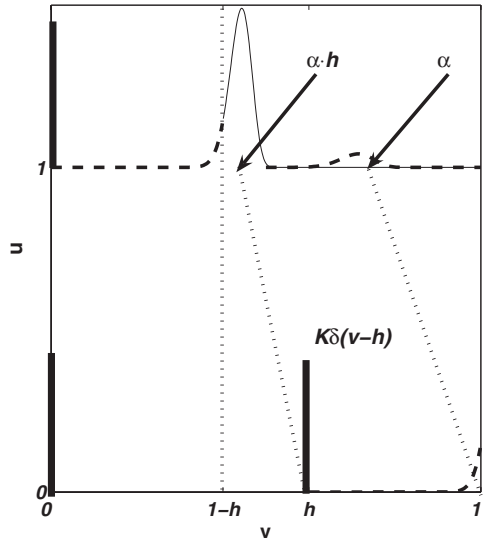

Figure 5: Heuristic analysis. The net flux for $v > 1 - h$, at $u = 1$, accounts for the LGN firing rate K. This appears as a delta function at $u = 0$, $v = 0$, as a heavy line, and since flux is conserved at $v = 0$, there is also a delta function of strength K at $u = 1$. This in turn produces the δ-function indicated at $v = h$. The last generates the smooth gaussian-like flux shown at $u = 1$. The flux at $u = 1$ for $v > 1 - h$ contributes spiking ratio 2 firing to K, and the $v < 1 - h$ dashed curve, right, translates by h to $u = 0$ as shown, and then appears at $u = 1$ for $v > 1 - h$ and contributes LGN firing at spiking ratio 3.

$sh/\gamma = .84$, the delta function is quite small (note the diminished vertical scale), and we are in a regime for which $sh/\gamma < 1$, so that deterministically, the LGN would not fire. For the deterministic analog of this last case, we encountered an attracting limit cycle,

$$sh/\gamma = \underline{v}_\infty \rightleftarrows \bar{v}_\infty = \left(1 - \frac{\gamma}{s}\right)\frac{sh}{\gamma}, \tag{5.16}$$

and no LGN firing. The frame in the lower right of Figure 6 indicates that the limit cycle, equation 5.16, now appears as a diffusely spread region, enough so that it produces a small level of LGN firing.

6 Integral Equation Formulation

For small μ, equation 5.15 provides an accurate approximation for the Green's function which we now use to reduce the problem to an integral equation.

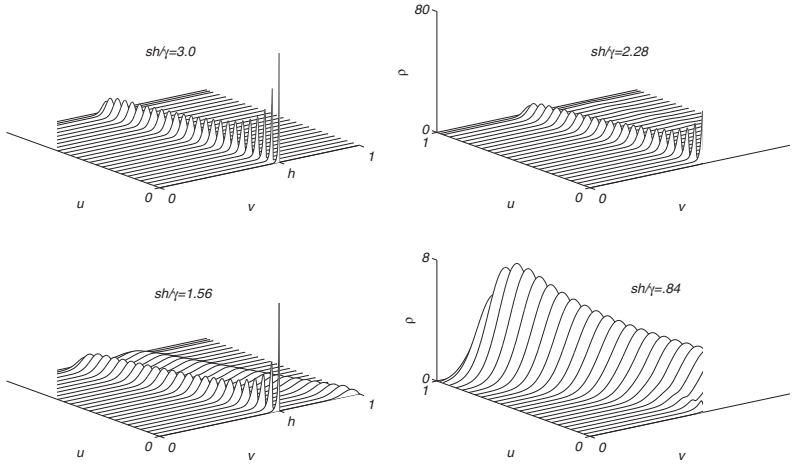

Figure 6: Exact computations based on equation 6.7. In all cases $h = h_v = .6$, $\gamma^{-1} = 50$ msec and $h_u = .03$. The strength of the delta function at $u = 0$, $v = h$, is K. An extra plot has been inserted near $u = 1$ to indicate that the density falls to zero at $u = 1$. Note that the vertical plot scales vary.

Up to a multiplicative constant, which we fix later, we express the exiting flux at $u = 1$ by

$$J(u = 1, v) = \psi(v) + \delta(v) \int_{1-h}^{1} \psi(v')\, dv', \tag{6.1}$$

where the second term on the right of equation 6.1 specifies that the input flux at the origin comes from the integrated flux leaving the last subinterval at $u = 1$. From the boundary condition, equation 4.7, the incoming flux at $u = 0$ (excluding the flux at $v = 0$) is then

$$\hat{J}(u = 0, v) = \psi(v - h) + \int_{1-h}^{1} \psi(v')\, dv' \delta(v - h) \approx s\hat{\rho}(0, v), \tag{6.2}$$

where the approximation on the right-hand side of equation 6.2 follows from the smallness of μ. From this and the Green's function, equation 5.15, it follows that

$$\begin{aligned} \hat{\rho}(u, v) &= \phi(u) \int_{h}^{1} D(u, v : v_0) \hat{\rho}(0, v_0)\, dv_0 \\ &= \frac{\phi(u)}{s} \left\{ \int_{1-h}^{1} \psi(v')\, dv' D(u, v : h) + \int_{0}^{1-h} D(u, v : v' + h) \psi(v')\, dv' \right\}. \end{aligned} \tag{6.3}$$

Next, we use equation 5.3, $-\mu \frac{\partial \phi}{\partial u}|_{u=1} = s$, to calculate $\hat{f}(u = 1, v)$, which for $v > 0$ is just $\psi(v)$ and hence,

$$\psi(v) = \int_0^{1-h} D(1, v : v' + h)\psi(v')dv' + D(1, v : h)\int_{1-h}^{1} \psi(v')dv = L\psi, \tag{6.4}$$

which is the desired integral equation.[1]

Equation 6.4 can be regarded as an eigenfunction problem with unit eigenvalue. The presence of a unit eigenvalue is confirmed by the fact that $\tilde{\psi} = 1$ is an eigenfunction of the adjoint, $L^{\dagger}$, with unit eigenvalue. Equation 6.4 also has the interpretation that ψ is an admixture of $D(1, v, v')$ for $v' \geq h$.

It still remains for us to appropriately normalize the eigenfunction $\psi(v)$. Toward this end we write the appropriate solution as

$$\Psi(v) = C\psi(v), \tag{6.5}$$

then instead of equation 6.1, we have

$$J(u = 1, v) = C\left(\psi(v) + \int_{1-h}^{1} \psi(v')\,dv'\delta(v)\right) \tag{6.6}$$

and since the net flux at $u = 1$ is just the RGC firing rate J_o, it follows that the solution for the exiting flux for $v > 0$, at $u = 1$, is given by

$$\Psi(v) = \frac{J_o\psi(v)}{\int_0^1 \psi(v')\,dv' + \int_{1-h}^{1} \psi(v')\,dv'}, \tag{6.7}$$

and hence that the transfer ratio is

$$\frac{K}{J_o} = \frac{\int_{1-h}^{1} J_o\psi(v')\,dv'}{\int_0^1 \psi(v')\,dv' + \int_{1-h}^{1} \psi.(v')\,dv'}. \tag{6.8}$$

It is clear from equation 6.8 that for relatively small current $K/J \to 0$, while for large currents $K/J_o \to 1/2$.

[1] If equation 6.4 is formally written as $(1 - T)\psi = D(1, v : h)$, then the iteration procedure sketched in the previous section yields the first few terms of the Neumann series, $\psi = (\sum_{n=0}^{\infty} T^n)D(1, v : h)$.

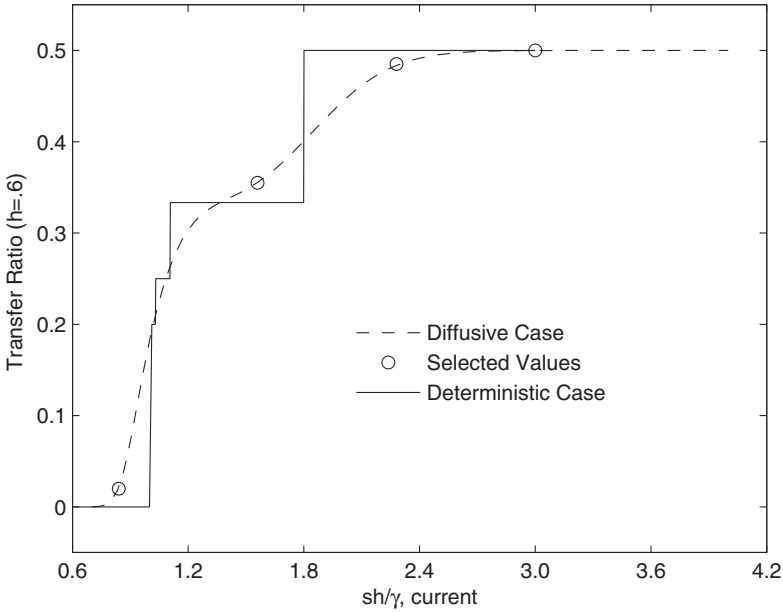

Figure 7: The transfer ratio, K/J_o, as given by equation 6.8, for $\gamma = 20/\text{sec}$ and $h = .6$, is plotted as a dashed line, which contrasts with equation 3.17, the unbroken line. Circles show the four selected values shown in Figures 6 and 8.

Equation 6.4 was directly discretized and solved numerically. With the solution 6.7 known, equation 6.6 gives $\hat{J}(v)$ and equation 6.3 furnishes $\hat{\rho}(u, v)$. Figure 8 exhibits a range of solutions of $\psi(v)$, for $3 \geq sh/\gamma \geq .84$, with $\gamma^{-1} = 50$ msec and $h = .6$. Note that these correspond to the four solutions for $\hat{\rho}(u, v)$, arising from equation 6.3, that are depicted in Figure 6. At the highest value, $sh/\gamma = 3$, the delta function at $u = 0$, $v = h$, diffuses into a near gaussian at $v = (1 - \gamma/s)h$, well to the right of $v = 1 - h$. As indicated in Figure 7, the spike ratio is almost 2 and explains why the corresponding plot in Figure 6 does not show bimodality. At the next value, $sh/\gamma = 2.28$, in Figure 8, the diffused delta function straddles $v = 1 - h$, with most of the gaussian to the right of $v = 1 - h$, so that most LGN firings corresponded to the spike ratio of 2, with a smaller fraction having a spike ratio of 3 (see Figure 5), and from Figure 7 we see the spiking ratio is 2.1 in case. The reverse situation is seen for $sh/\gamma = 1.56$, where the spike ratio is 2.8. Finally for $sh/\gamma = .84$ the peak lies at $v = \bar{v}_\infty = \frac{sh}{\gamma} - h$, corresponding to the location of the limiting cycle. In this last case as seen from Figure 7, the RGC is mainly shooting blanks, since the spiking ratio is 50.

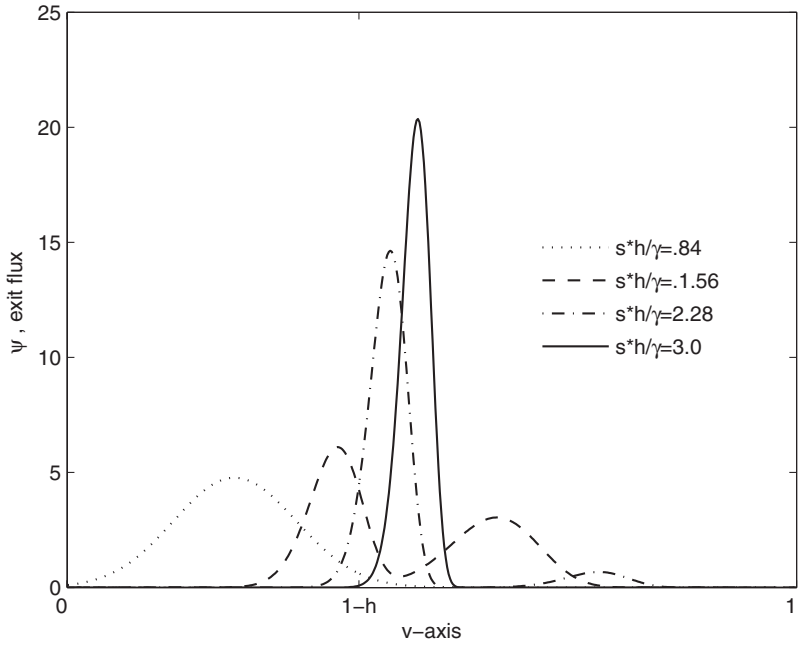

Figure 8: Range of solutions, ψ normalized to have a unit integral, for $\gamma^{-1} = 50$ msec and $h = .6$. Each case shown has a transfer ratio shown on Figure 7.

7 Summary and Discussion

Insight into the workings of the RGC/LGN system, along with clear-cut criteria, was gained by examining the deterministic (nonstochastic) version of the RGC/LGN system, equations 2.1 and 2.2. Within this framework, the retinal ganglion cells do not spike unless the incoming average current, s, exceeds leakage $s/\gamma > 1$. Moreover, even if the RGC spikes, no LGN spiking is present unless $sh/\gamma > 1$, that is, S-potential bumps, h, must be large enough. Even when sh/γ exceeds unity, many arrivals may be necessary for an LGN spike; that is, the transfer ratio can be very small. This is depicted in Figure 7 by the rectilinear plot, for the nominal value of $h = .6$. For this value of h, the transfer ratio does not reach the theoretically predicted maximum until $sh/\gamma \approx 3$. The dashed continuous curve in Figure 7 shows the blurring of the deterministic boundaries by the inclusion of stochasticity in the theoretical model.

The theoretical model was obtained by regarding the RGC/LGN as a single dynamical system, thus preserving precise firing, and then placing this dynamical system within a population framework, resulting in equations 2.3 (or 2.15) and 2.16 in the diffusive approximation. An approximate

solution of this model, for small diffusivity in the case of equilibrium, sections 4 and 5 revealed that the deterministic picture serves as a scaffolding, which stochasticity adorns with diffusion and a boundary layer. Moreover, the deterministic discreteness of the transfer ratio transforms to a collection of substates that have different transfer ratios resulting in an average value, as depicted in Figure 7.

Finally, through good fortune, we obtained a highly accurate form of the Green's function for the problem in the limit of small diffusivity. This was applied in section 6 to reduce the solution of the problem to an integral equation that could be treated numerically with ease. Figure 6 exhibits a range of solutions, $\hat{\rho}(u, v)$, and Figure 8 a corresponding range of exit fluxes (and hence firing rates), based on sh/γ, obtained from the solution of the integral equation. In all cases, the area under each curve indicates the RGC firing rate, and the area to the right of $1 - h$, the corresponding LGN firing rate. The transfer ratios for the depicted cases are shown as circles on Figure 7.

The model presented in this letter rests on accepted and tested neuronal mechanisms and was developed within the framework of an experimentally determined wiring diagram. Within the framework of the model, the issue of "editing by the LGN" takes on a differing perspective. Instead of some elaborate or sophisticated circuitry designed to extract or verify information, the model suggests that relay cells have been designed to fire mainly when they receive at least two arrivals within a short enough interval of time that is determined by leakage. Note that the relay cell leakage time has been estimated at 10 msec (Ozaki & Kaplan, 2006), a factor of five shorter than the estimated RGC leakage time of 50 msec (Fohlmeister & Miller, 1997). Some modification of the view expressed may be necessary when we better know the nature and role of other inputs to relay cells.

A further feature of the formalism is the inclusion of the stochasticity that is implicit in the population approach. Although not carried out here, a further source of stochasticity is variation in synaptic arrival strength; which may be implemented, with a probability distribution in jump size h (Omurtag, Knight, et al., 2000). As mentioned earlier, our model can be further enriched by including additional interactive populations that reflect the known wiring diagram. A brief example of this, which includes a brainstem input, is presented in the appendix and briefly discussed below.

A desirable, if not essential, feature of any model is that it be predictive (and falsifiable; Popper, 2002), which is a feature of the model proposed here (see Hayot & Tranchina, 2001, for a another approach). In this connection mention should be made of the recent series of models (Pillow & Simoncelli, 2006); Pillow, Paninski, Uzzell, Simoncelli, & Chichilnisky, 2005; Jolivet, Lewis, & Gerstner, 2004; Schwartz, Pillow, Rust, & Simoncelli, 2006; Keat, Reinagel, & Reid, 2001; Casti et al., 2007) for RGC and RGC/LGN responses that reflect a different point of view. These models are largely based on mathematical and statistical structures, in contrast to the more biologically

based model of this letter. A further contrast with the formulation here is that these models are usually trained by experimental data to become predictive tools. Application of such methods to response behavior of our model might provide a revealing sources of information from a different perspective.

7.1 Extension of the Model. A result of the analysis presented here is that for $h_v < 1$, the transfer ratio is never greater than $1/2$ or, alternatively, at least two RGC spikes are necessary for an LGN spike. As Figure 2 suggests, S-potentials are below threshold. (Since Figure 2 is an extracellular recording, it does not reliably estimate h_v.)

This point is of some importance since the transfer ratio is known to sometimes rise above .5 but always remains below unity (Andolina et al. 2007; Sincich et al., 2007; Ozaki & Kaplan, 2006). Close examination of Figure 2 shows small, persistent bumps that are not recorded as S-potential arrivals. If these represent poorly resolved RGC arrivals, then this might alter the calculated transfer ratios. Finally, it should be noted that the analysis applies only to equilibrium and that unsteadiness will lead to new phenomena. Ozaki and Kaplan (2006) persuasively demonstrate that an area of the brainstem, the parabrachial nucleus (PBN), effects LGN activity and that this affect is globally felt in the LGN so that, consistent with our model, for intermittent periods, PBN activity transfer ratios could rise above .5. Such results were demonstrated under spontaneous fluctuations and were also shown by electrical stimulation of the PBN. The appendix contains a discussion of how the model might be modified to treat this case.

Appendix: Details and Extensions of the Model

A.1 Detailed Two-Neuron Equations. If equation 2.4 is substituted into equation 2.3, we obtain

$$\begin{aligned}\frac{\partial \rho(u,v,t)}{\partial t} &= \frac{\partial}{\partial u}(\gamma_u u \rho) + \frac{\partial}{\partial v}(\gamma_v v \rho) + \sigma(t)\{\rho(u-h_u,v) - \rho(u,v)\} \\ &\quad + \sigma(t)\delta(u)\int_{1-h_u}^{1} du'\rho(u,v-h_v,t)\,du' + \sigma(t)\delta(u)\delta(v) \\ &\quad \times \int_{1-h_u}^{1} du' \int_{1-h_v}^{1} dv'\rho(u',v',t). \qquad \text{(A.1)}\end{aligned}$$

If equation 2.11 is substituted into A.1, we obtain the following coupled system of equations for describing the RGC/LGN interaction:

$$\begin{aligned}\frac{\partial A}{\partial t} &= \frac{\partial}{\partial v}(\gamma_v v A) - \sigma(t)A + \sigma(t)\{\delta(v-h_v)\int_{1-h_u}^{1} B(u',t)\,du' \\ &\quad + \int_{1-h_u}^{1} du'\hat{\rho}(u',v-h_v,t)\}\end{aligned}$$

$$\frac{\partial B}{\partial t} = \frac{\partial}{\partial u}(\gamma_u u B) + \sigma(t)\{B(u - h_u t) - B(u,t)\} + \sigma(t)C(t)\delta(u - h_u)$$
$$\frac{\partial C}{\partial t} = -\sigma(t)C + \sigma(t)\int_{1-h_u}^{1} du' \int_{1-h_v}^{1} dv' \hat{\rho}(u', v', t)$$
$$\frac{\partial \hat{\rho}}{\partial t} = \frac{\partial}{\partial u}(\gamma_u u \hat{\rho}) + \frac{\partial}{\partial v}(\gamma_v v \hat{\rho}) + \sigma(t)\{\hat{\rho}(u - h_u, v, t) - \hat{\rho}(u, v, t)\}$$
$$+ \sigma(t) A(v,t)\delta(u - h_u). \tag{A.2}$$

It is clear from equation A.2 that B and $\hat{\rho}$ have discontinuities at $u = h_u$ and that $A(v,t)$ has one at $v = h_v$.

A.2 RGC/LGN/PBN Model. As discussed in the main text the experiments of Ozaki and Kaplan (2006) suggest that an external PBN current to the LGN relay cells can play an important role. To account for this, and in the absence of any knowledge about PBN circuitry, we might account for this by replacing equation 3.2 by

$$\frac{dv}{dt} = -\gamma v + h\sum \delta(t - \tau_j) + h_B \sum \delta\big(t - \tau_j^B\big), \tag{A.3}$$

where $\{\tau_j^B\}$ denote PBN arrival times and h_B the corresponding membrane potential jumps. Within the deterministic framework of section 3, the times $\{\tau_j\}$ are set by the $u = 1$ exit times. By contrast, $\{\tau_j^B\}$ are externally set, and at such times, the trajectory in the unit square makes a horizontal leap h_B to the right.

Depending on the frequency of PBN arrivals, $\tau_B(t)$, and the magnitude of h_B, a variety of possibilities can occur. A single RGC arrival can produce an LGN firing, and LGN firings can now also occur with trajectories leaving the square at $v = 1$. To include the presence of a PBN current, in the population equation we replace J_v in equation 2.3 by

$$J_v = -\gamma_v v \rho(u, v, t) + \sigma_B(t)\int_{v-h_B}^{v} \rho(u, v', t)\, dv' \tag{A.4}$$

and add the source term

$$\sigma_B(t)\int_{1-h_B}^{1} \rho(u, v', t)\, dv' \delta(v) \tag{A.5}$$

to the right-hand side of equation 2.3. Equation A.5 deals with the feature that there is now a flux of neurons that leaves the square at $v = 1$ and reappears at $v = 0$.

Acknowledgments

During the course of the research reported here, I was fortunate to have the advice and help of Bruce W. Knight. This interaction played a key role, and I deemed it appropriate to include Professor Knight as a coauthor, an offer he generously declined. It is therefore with great pleasure and gratitude that I acknowledge Bruce Knight for his unselfish help and suggestions. I am also grateful to Ehud Kaplan for sharing his basic insights on this problem and his helpful comments. Mention must also be made of the two very fine referees and their excellent suggestions. Support for this work came from NIH/NEI EY16224 and NIH/GM071558.

References

Amit, D., & Brunel, N. (1997). Dynamics of a recurrent network of spiking neurons before and following learning. *Network*, *8*, 373–404.

Andolina, I., Jones, H., Wang, W., & Sillito, A. (2007). Corticothalamic feedback enhances stimulus response precision in the visual system. *Proc. Natl. Acad. Sci.*, *104*, 1685–1690.

Bishop, P. (1953). Synaptic transmission: An analysis of the electrical activity of the lateral geniculate nucleus in the cat after optic nerve stimulation. *Proc. R. Soc. Lond. B, Biol. Sci.*, *141*, 362–392.

Brunel, N., & Hakim, V. (1999). Fast global oscillations in networks of integrate-and-fire neurons with low firing rates. *Neural Computation*, *11*, 1621–1671.

Casti, A., Hayot, F., Xiao, Y., & Kaplan, K. (in press). A simple model of retinal-LGN transmission. *Journal of Computational Neuroscience*.

Casti, A., Omurtag, A., Sornborger, A., Kaplan, E., Knight, B., Victor, J., et al. (2002). A population study of integrate-and-fire-or-burst neurons. *Neural Comp.*, *14*, 957–986.

Cleland, B., Dubin, M., & Levick, W. (1971a). Simultaneous recording of input and output of lateral geniculate nucleus. *Nat. New Biol.*, *231*, 191–192.

Cleland, B., Dubin, M., & Levick, W. (1971b). Sustained and transient neurons in the cat's retina and lateral geniculate nucleus. *J. Physiol.*, *217*, 473–496.

Cole, J. (1968). *Perturbation methods in applied mathematics*. New York: Blaisdell Publishing.

Cucchiaro, J., Uhlrich, D., & Sherman, S. (1988). Parabrachial innervation of the cat's dorsal lateral geniculate nucleus: An electron microscopic study using the tracer Phaseolus vulgaris Leucoagglutinin (PHA-L). *J. Neurosci.*, *8*, 4576–4588.

Dowling, J. (1992). *Neurons and networks: An introduction to neuroscience*. Cambridge, MA: Belknap Press.

Einstein, A. (1905). Motion of suspended particles in stationary liquids required from the molecular kinetic theory of heat. *Annalen der Physik*, *17*, 549–560.

Fohlmeister, J., & Miller, R. (1997). Impulse encoding mechanisms of ganglion cells in the tiger salamander retina. *J. Neurophysiol.*, *78*, 1935–1947.

Fourcaud, N., & Brunel, N. (2002). Dynamics of the firing probability of noisy integrate-and-fire neurons. *Neural Computation*, *14*, 2057–2110.

Freed, M. (2005). Quantal encoding of information in a retinal ganglion cell. *J. Neurophysiol.*, *94*, 1048–1056.

Fusi, S., & Mattia, M. (1999). Collective behavior of networks with linear (VLSI) integrate-and-fire neurons. *Neural Computation*, *11*, 633–652.

Gardiner, C. (2005). *Handbook of stochastic methods*. Berlin: Springer-Verlag.

Gerstner, W. (1995). Time structure of the activity in neural network models. *PRE*, *51*, 738–758.

Gerstner, W., & Kistler, W. (2002). *Spiking neuron models*. Cambridge: Cambridge University Press.

Gerstner, W., van Hemmen, J., & Cowan, J. (1996). What matters in neuronal locking? *NCOMP*, *8*, 1653–1676.

Haskell, E., Nykamp, D., & Tranchina, D. (2001). Population density methods for large-scale modeling of neuronal networks with realistic synaptic kinetics: Cutting the dimension down to size. *Network: Comput. Neural Syst.*, *12*, 141–174.

Hayot, F., & Tranchina, D. (2001). Modeling the sensitivity of lateral geniculate neurons to orientation discontinuity and the role of feedback from visual cortex. *Visual Neurosci.*, *85*, 865–877.

Jolivet, R., Lewis, T., & Gerstner, W. (2004). Generalized integrate-and-fire models of neuronal activity approximate spike trains of a detailed model to a high degree of accuracy. *J. Neurophysiol.*, *92*, 959–976.

Kaplan, E., & Shapley, R. (1984). The origin of the S (slow) potential in the mammalian lateral geniculate nucleus. *Exp. Brain Res.*, *55*, 111–116.

Keat, J., Reinagel, P., & Reid, R. (2001). Predicting every spike: A model for the responses of visual neurons. *Neuron*, *30*, 803–817.

Kistler, W., Gerstner, W., & van Hemmen, J. (1997). Reduction of the Hodgkin-Huxley equation to a single-variable threshold model. *Neural Comp.*, *9*, 1015–1045.

Knight, B. (2000). Dynamics of encoding in neuron populations: Some general mathematical features. *Neural Computation*, *12*, 473–518.

Knight, B., Manin, D., & Sirovich, L. (1996). Dynamical models of interacting neuron populations. In E. C. Gerf (Ed.), *Symposium on Robotics and Cybernetics: Computational Engineering in Systems Applications.* Lille, France: Cite Scientifique.

Knight, B., Omurtag, A., & Sirovich, L. (2000). Dynamics of neuronal populations: Analytic solution of step-transient response compared to direct simulation. *Neural Computation*, *12*, 1045–1055.

Koch, K., McLean, J., Berry, M., Sterling, P., Balasubramanian, V., & Freed, M. (2004). Efficiency of information transmission by retinal genglion cells. *Current Biology*, *14*, 1523–1530.

Langevin, P. (1906). Sur la théorie du mouvement brownien. *Comptes Rendus Acad. Sci.*, *146*, 530–633.

Levick, W., Cleland, B., & Dubin, M. (1972). Lateral geniculate neurons of cat: Retinal inputs and physiology. *Invest. Ophthalmol.*, *11*, 302–311.

Lytton, W., & Sejnowski, T. (1991). Simulations of cortical pyramidal neurons synchronized by inhibitory interneurons. *J. Neurophysiol.*, *66*, 1059–1079.

Mattia, M., & Del Giudice, P. (2002). Population dynamics of interacting spiking neurons. *Phys. Rev. E.*, *66*, 051917.

McCormick, D., & Huguenard, J. (1992). A model of the electrophysiological properties of thalamocortical relay neurons. *J. Neurosci.*, *68*, 1384–1400.

Mumford, D. (1991). On the computational architecture of the neo-cortex I. The role of the thalamocortical loop. *Biol. Cybern.*, *65*, 135–145.

Nykamp, D., & Tranchina, D. (2000). A population density approach that facilitates large-scale modeling of neural networks: Analysis and an application to orientation tuning. *J. Comp. Neurosci.*, *8*, 19–50.

Omurtag, A., Kaplan, E., Knight, B., & Sirovich, L. (2000). A population approach to cortical dynamics with an application to orientation tuning. *Network*, *11*, 247–260.

Omurtag, A., Knight, B., & Sirovich, L. (2000). On the simulation of large populations of neurons. *J. Comp. Neurosci.*, *8*, 51–63.

Ozaki, T., & Kaplan, E. (2006). Brainstem input modulates globally the transmission through the lateral geniculate nucleus. *Intern. J. Neuroscience*, *116*, 247–264.

Pillow, J., Paninski, L., Uzzell, V., Simoncelli, E., & Chichilnisky, E. (2005). Prediction and decoding of retinal ganglion cell responses with a probabilistic spiking model. *J. Neuroscience*, *25*, 11003–11013.

Pillow, J., & Simoncelli, E. (2006). Dimensionality reduction in neural models: An information-theoretic generalization of spike-triggered average and covariance analysis. *Journal of Vision*, *6*, 414–428.

Popper, K. (2002). *The logic of scientific discovery*. New York: Routledge.

Rieke, F., Warland, D., van Steveninck, R., & Bialek, W. (1997). *Spikes: Exploring the neural code*. Cambridge, MA: MIT Press.

Risken, H. (1996). *The Fokker-Planck equation: Methods of solution and applications*. Berlin: Springer-Verlag.

Ritz, R., & Sejnowski, T. (1997). Synchronous oscillatory activity in sensory systems: New vistas on mechanisms. *Current Opinion in Neurobiol.*, *7*, 536–546.

Ruksenas, O., Fjeld, I., & Heggelund, P. (2000). Spatial summation and center-surround antagonism in the receptive field of single units in the dorsal lateral geniculate nucleus of cat: Comparison with retinal input. *Visual Neuroscience*, *17*, 855–870.

Schwartz, O., Pillow, J., Rust, N., & Simoncelli, E. (2006). Spike-triggered neural characterization. *Journal of Vision*, *6*, 484–507.

Sherman, S., & Guillery, R. (1996). The functional organization of thalamocortical relays. *J. Neurophysiol.*, *76*, 1367–1395.

Sincich, L., Adams, D., Economides, J., & Horton, J. (2007). Transmission of spike trains at the retinogeniculate synapse. *J. Neurosci.*, *27*, 2683–2692.

Sirovich, L. (2003). Dynamics of neuronal populations: Eigenfunction theory; some solvable cases. *Network: Comput. Neural Syst.*, *14*, 249–272.

Sirovich, L., Knight, B., & Omurtag, A. (2000). Dynamics of neuronal populations: The equilibrium solution. *SIAM J. Appl. Math.*, *60*, 2009–2028.

Sirovich, L., Omurtag, A., & Lubliner, K. (2006). Dynamics of neural populations: Stability and synchrony. *Network: Comput. Neural Syst.*, *17*, 3–29.

Stein, R. (1965). A theoretical analysis of neuronal variability. *Biophys. J.*, *5*, 173–194.

Uhlrich, D., Cucchiaro, J., Humphrey, A., & Sherman, M. (1991). Morphology and axonal projections patterns of individual neurons in the cat perigeniculate nucleus. *J. Neurophysiol.*, *65*, 1528–1541.

Uhlrich, D., Cucchiaro, J., & Sherman, M. (1988). The projection of individual axons from the parabrachial region of the brain stem to the dorsal lateral geniculate nucleus of the cat. *J. Neurosci.*, *8*, 4565–4575.

Usrey, W., & Reid, R. (1999). Synchronous activity in the visual system. *Annu. Rev. Physiol.*, *61*, 435–456.

Usrey, W., Reppas, J., & Reid, R. (1999). Specificity and strength of retinogeniculate connections. *J. Neurophysiol.*, *82*, 3527–3540.

Wilbur, W., & Rinzel, J. (1982). An analysis of Stein's model for stochastic neuronal excitation. *Biol. Cybern.*, *45*, 107–114.

Wilbur, W., & Rinzel, J. (1983). A theoretical basis for large coefficient of variation and bimodality in neuronal interspike interval distributions. *J. Theor. Biol.*, *105*, 345–368.

Wilson, H., & Cowan, J. (1973). A mathematical theory of the functional dynamics of cortical and thalamic nervous tissue. *Kybernetik*, *13*, 55–80.

Received March 1, 2007; accepted May 31, 2007.